JOURNAL OF GUIDANCE, CONTROL, AND DYNAMICS
Vol. 20, No. 4, July–August 1997

Bifurcation Analysis of a Highly Augmented Aircraft Model

Giulio Avanzini*
University of Rome "La Sapienza," Rome 00184, Italy
and
Guido de Matteis†
Polytechnic of Turin, Turin 10129, Italy

Bifurcation theory is used to analyze the dynamics of a modern high-performance aircraft. An F-16 fighter aircraft model, which includes a full-authority control system, is considered. The vehicle is a basically unstable configuration, and its response modes are tailored by the flight control system according to different mission tasks. The steady states of the F-16 are computed by a numerical continuation method. The classical application of this technique to trace the steady states of the system as continuous functions of control deflections or control force is to be reconsidered when the use of maneuver demand control in highly augmented aircraft provides zero stick force for most of the trimmed flight conditions of the vehicle. The practical worth of bifurcation theory for the design and analysis of high-performance aircraft is evaluated. Such aspects of the problem as the selection of meaningful parameters for the continuation procedure and the interpretation of the bifurcation diagrams are discussed for the different modes of operation of the flight control system. The behavior of the aircraft model at high angle of attack is predicted when the alpha limiter is disengaged to simulate the effects of possible failure conditions.

Nomenclature

a_n	= normal load factor
a_y	= lateral load factor
$\|\boldsymbol{b}\|_P$	= $\max_{i=1}^{n} \|b_i\|$
$\|\boldsymbol{b}\|_T$	= $\|b_1\| + \|b_2\| + \cdots + \|b_n\|$
$\bar{c}$	= mean aerodynamic chord
F_{lat}	= lateral stick force
F_{long}	= longitudinal stick force
F_{ped}	= pedal force
g_{com}	= incremental load factor
H_e	= engine angular momentum
h	= altitude
M	= Mach number
P_e	= power level
p, q, r	= roll, pitch, and yaw velocity, respectively
$\boldsymbol{u}$	= control vector
V	= flight speed
$\boldsymbol{x}$	= state vector
α	= angle of attack
β	= sideslip angle
γ	= flight-path angle
δ_A	= aileron angle
δ_D	= differential stabilator angle
δ_E	= symmetric stabilator angle
$\delta_{E_l}, \delta_{E_r}$	= left and right stabilator angle, respectively
δ_R	= rudder angle
δ_T	= commanded thrust level
χ, θ, ψ	= Euler angles
Ω	= turn rate

I. Introduction

In the last 15 years, dynamical system theory (DST)[1] has provided a powerful tool for the analysis of nonlinear phenomena in aircraft behavior. In the applications of DST, numerical continuation methods[2] and bifurcation theory[1] have been used to study roll-coupling instabilities and stall/spin phenomena of a number of aircraft models, including F-4, Alpha Jet, F-14, and F-15 fighters. Results of great interest have been reported in several papers, and in the recent study by Jahnke and Culick,[3] the theoretical background of this technique is recalled and a rather complete review of the relevant investigations in the field is presented.

Since the first application of DST to the nonlinear stability of aircraft in the work by Carrol and Mehra,[4] which was focused on the underlying principles of bifurcation analysis and was intended to demonstrate the great value of this methodology in providing qualitative information on high-α phenomena, most of the studies in the literature have dealt with basic airframe models where stability and/or control augmentation systems (SCAS or CAS) are absent. This approach, when statically stable aircraft are considered, allows for the dynamics of the unaugmented model to be characterized and, as a possible further step, the effect of simple CAS schemes on the baseline motions to be analyzed.

To the authors' knowledge, in only one case were control augmentation and control dynamics, including pitch, roll, and yaw CAS, added to a basic F-15 model[5] to carry out a more realistic and complete investigation of the aircraft behavior at high incidence. Continuation diagrams in terms of longitudinal and lateral stick forces and rudder pedal force showed that the qualitative structure of the steady states was hardly modified by the CAS, whereas noticeable effects on motion amplitudes were evident.

In the last two decades, multiple redundant, full authority, fail/operational, fly-by-wire control systems have been brought to a very mature state. As a result, many aircraft, from earlier designs such as the F-16, F-18, and Tornado through the more recent Mirage 2000, European Fighter Aircraft (EFA), Rafale, and advanced demonstrators such as X-29 and X-31, are highly augmented, actively controlled vehicles that possess a negative or marginal static stability without augmentation, for reasons related to improved performances, weight/cost reduction, and/or low observability.[6] Highly augmented and/or superaugmented aircraft present dynamic characteristics that are markedly different, in the qualitative nature of the steady states, as compared to the basic airframes alone.

In this paper, the dynamics of a relaxed stability aircraft is analyzed by DST. The principal objective of the study is to assess the practical worth of this technique in situations where the dynamics of the vehicle are tailored by the full-authority control system according to different mission tasks. We also remark that the use of maneuver demand control in high-performance aircraft somehow limits the capability of DST to provide global stability information inasmuch as transient motions cannot be predicted or quantified by bifurcation theory.[4]

Presented as Paper 96-3367 at the AIAA Atmospheric Flight Mechanics Conference, July 29–31, 1996; received Sept. 3, 1996; revision received March 19, 1997; accepted for publication March 20, 1997.

*Ph.D. Student, Department of Mechanics and Aeronautics, Via Eudossiana 18.

†Professor, Department of Aerospace Engineering, Corso Duca degli Abruzzi 24. Member AIAA.

When reference is made to the reported applications of DST,[3–5] certain additional problems are faced, the solutions of which are as straightforward as, for instance, the modeling of the SCAS with the related high number of additional states and the handling of the so-called breakpoint nonlinearities coming from control system elements such as gain schedules, limiters, and deadbands, which generate discontinuous derivatives. On the other hand, some aspects of the procedure of analysis are of great interest when, for instance, we note that a neutral stick force gradient with speed is inherently provided, depending on the SCAS mode of operation. As a consequence, aspects of the problem such as the selection of meaningful parameters for the continuation analysis and the interpretation of the results corresponding to the different SCAS modes are worth a careful and detailed evaluation.

Then, such circumstances are brought into consideration when one of the SCAS subsystems is not active. This kind of approach may simulate the effects of possible failure conditions or can be used to analyze equilibrium states that are not allowed by the SCAS in normal operations. For instance, once an existing alpha limiter is disengaged, a prediction of the vehicle dynamics at high incidence is accomplished that can eventually lead to an improvement of the performance in maneuvering flight.

In our application, we consider the low-speed model of the F-16 single-seat, single-engine fighter aircraft,[7] which includes a full authority, fly-by-wire flight control system featuring a sidestick controller and a high-gain aerodynamic α–δ_E feedback to counter the slight instability in pitch of the basic airframe.[8] Although the modeled SCAS is relatively dated, it incorporates several elements featured by the actual flight control systems of highly augmented aircraft and appears realistic enough and not too complex for the purposes of the present study.

The theoretical background of this study is reported in Sec. II, where the principal features of the aircraft model, including the SCAS, are provided and the relevant aspects of the bifurcation analysis are recalled. In Sec. III, significant bifurcation diagrams related to the different SCAS modes of operation are presented and discussed. A section of conclusions ends the paper.

II. Analysis

The full, nonlinear set of motion equations for the rigid aircraft is written in body axes $\mathcal{F}_B$ in terms of the velocity components u, v, and w, angular rates p, q, and r, and Euler angles χ, θ, and ψ, as in Ref. 7. The model accounts for the gyroscopic effects of the single engine through a constant angular momentum H_e along the longitudinal axis. The engine dynamics and response to the throttle δ_T are simulated by a first-order lag, which depends on the power level P_e. For $P_e \geq 0.5P_{e_{\max}}$, to which $\delta_T \geq 0.77$ corresponds, the afterburner is on. The F-16 model includes second-order lag dynamics for a full-span leading-edge flap. As a consequence of the yaw angle being an uncoupled variable, the basic, unaugmented model is an 11th-order system.

Control System Model

The principal features of the aircraft SCAS, the details of which are reported in Refs. 7–9, are recalled in this subsection. A schematic of the control system model is shown in Fig. 1. The primary aerodynamic control system has symmetric stabilators for pitch control, wing-mounted flaperons and differential stabilators for roll control, and a conventional rudder for yaw control. The leading-edge flap deflection is scheduled as a function of angle of attack and Mach number. Force-sensing sidestick controller and force-sensing rudder pedals are modeled.

The longitudinal SCAS can operate in a g-response, pitch control mode for gross maneuvering capability and in an α-response mode for accurate path tracking. A third, q command, mode of operation has been implemented in the model to account for the properties of a reference, simple superaugmentation system[10] in the original F-16 model. As shown in Fig. 2, the pitch rate command mode was realized, as proposed in Ref. 9, by eliminating the feedback signal of normal acceleration while maintaining the α feedback for enhanced stability. Additionally, the washout filter in the pitch rate channel was maintained to avoid degradation in the

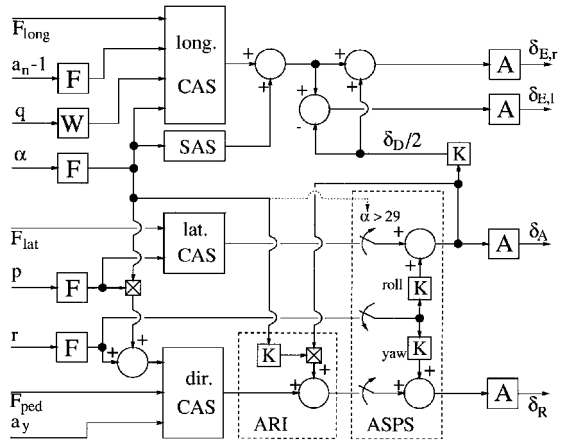

Fig. 1 F-16 control system logic: F, simple lag filter; W, wash-out filter; A, actuator dynamics; and K, scheduled gain.

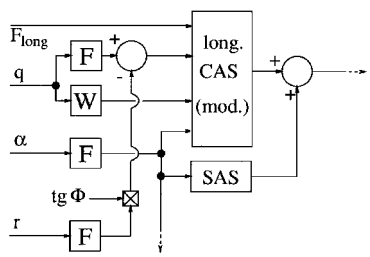

Fig. 2 Longitudinal control system logic for the q-command mode of operation.

α-limiter performance, and a stabilator compensation in steady turns, proportional to $r \tan \chi$, was allowed.[10]

A forward-loop integration is used to make the steady-state longitudinal response match the commanded input. Angle-of-attack and normal-acceleration limiting systems are provided by the longitudinal control system. The former system uses both α and q feedback loops to keep the angle of attack within the limit of 25 deg.

The lateral-directional control system includes a roll-rate augmentation system, a lateral acceleration-to-rudder feedback for augmented directional stability, a stability axis yaw-damper, and an aileron/rudder interconnect (ARI) to control the amount of coupling between the roll and yaw axes. An automatic departure/spin-prevention system (ASPS) is activated for $\alpha > 29$ deg to oppose any yaw-rate buildup using yaw-rate feedback on yaw and roll control surfaces. The complete model of the augmented aircraft is written in state-space form as

$$\dot{\boldsymbol{x}} = \boldsymbol{f}(\boldsymbol{x}, \boldsymbol{u}) \tag{1}$$

where the state and control vectors are, respectively, $\boldsymbol{x} \in \mathcal{R}^{33}$ and $\boldsymbol{u} = (F_{\text{long}}, F_{\text{lat}}, F_{\text{ped}}, \delta_T)^T \in \mathcal{R}^4$.

Aerodynamic Model

The aerodynamic model uses wind-tunnel data from low-speed ($M \leq 0.6$) static and dynamic tests conducted with subscale models of the F-16. In Ref. 7, static data are available in tabular form over the range $-20 \leq \alpha \leq 90$ deg and $-30 \leq \beta \leq 30$ deg, whereas dynamic data are provided for the same range of α.

The tabulated data are here expressed in the form of analytical functions, having a continuous first derivative, by cubic and bicubic interpolation[11] when the number of independent variables is one (α) or two (α, β), respectively. Terms depending on three variables, namely, (α, β, δ_E), are obtained by least-square polynomial fit and bicubic interpolation in terms of δ_E and (α, β), respectively. The described procedure led to a good accuracy in fitting the rather complex structures of the aerodynamic data, and, in particular, unwanted effects such as local curvatures introduced by the data smoothing were not observed. As a limitation, rotary balance data were not available in the F-16 aerodynamic model.

Bifurcation Analysis

It is our objective to discuss the particular aspects involved when DST is used to characterize the nonlinear dynamics of highly augmented aircraft. In short, bifurcation theory[1] requires the equilibrium points of the governing equations of the system to be evaluated and the stability of these states to be investigated. Here, a numerical continuation algorithm[2] is used for determining fixed points of the system (1), i.e., the solutions to the algebraic set

$$\boldsymbol{f}(\boldsymbol{x}_e, \boldsymbol{u}) = 0 \tag{2}$$

as the control variables, namely, the continuation or bifurcation parameters, are varied. In Eq. (2), the subscript e means at equilibrium. Once a solution $\tilde{\boldsymbol{x}}_e$ to Eq. (2) has been determined for a given value $\tilde{\boldsymbol{u}}$ of the control vector, the continuation algorithm allows one to calculate a new steady state for a perturbed value of the continuation variable. The procedure is divided into two steps because 1) a first estimate of the new equilibrium point is evaluated by a linear expansion of Eq. (2) in the neighborhood of the so-called starting solution $\tilde{\boldsymbol{x}}_e$ and 2) a Newton–Raphson algorithm is run until the convergence criteria

$$\frac{\left|\delta u_j^{(n)}\right|}{1 + \left|u_j^{(n)}\right|} < 10^{-4}, \qquad \frac{\left\|\delta \boldsymbol{x}^{(n)}\right\|_P}{1 + \left\|\boldsymbol{x}^{(n)}\right\|_P} < 10^{-4} \tag{3}$$

are satisfied, where $\delta u_j^{(n)}$ and $\delta \boldsymbol{x}^{(n)}$ are, respectively, the variation of continuation parameter and state vector at the nth iteration. This procedure is then iterated to trace a branch of steady states as a function of u_j.

After as many solution branches as possible have been calculated, i.e., the structure of equilibria for the considered model has been mapped, a local stability analysis is carried out by evaluating the eigenvalues of the system linearized about the steady states. The eigenvalues are computed using the module EIGRF of the International Mathematical and Statistical Libraries,[12] where the accuracy is expressed as

$$\frac{\|\boldsymbol{A}\boldsymbol{v}_j - \lambda_j \boldsymbol{v}_j\|_T}{N\|\boldsymbol{A}\|_T \|\boldsymbol{v}_j\|_T} < 10^{-6}$$

where λ_j and $\boldsymbol{v}_j$ are the jth eigenvalue and eigenvector, respectively, and N is the dimension of the Jacobian matrix $\boldsymbol{A}$.

Bifurcation points are identified along the branch using a secant method,[2] where the convergence criteria (3) are adopted. As a result, the location and nature of bifurcation points is determined in the bifurcation diagrams, where the states at equilibrium are plotted vs the continuation parameter. In this way a global, qualitative analysis of the aircraft behavior is realized.

At this point some general observations concerning the present application of DST are of interest. In the classic application of the continuation method to a basic airframe model, all of the control variables but one are fixed and the steady states are traced as a function of this variable. Then, the fixed points related to a given value of that parameter are used as starting points for computing the branches of equilibria when a different control parameter is varied. For instance, the unaugmented model of the F-16 has eight fixed points for $\delta_E = \delta_A = \delta_R = 0$, $\delta_T = 0.12$ to which four branches of steady states, evaluated having δ_A as the continuation parameter, correspond.

In highly augmented aircraft, variables associated with maneuvering states such as, for instance, q or the normal acceleration a_n, are directly commanded. Because of the proportional plus integral feedforward, the CAS provides zero tracking error for constant input and, consequently, most of the equilibrium conditions of the vehicle are realized at zero control force, i.e., zero value of the command parameter. When maneuver demand control is used, a nonzero stick force causes the aircraft to depart from equilibrium and determines a continuous variation of its state. It is only by releasing the stick that a new steady state is acquired. Because the continuation technique provides insight into steady-state behavior, the relation between the state of the aircraft and input command may not be revealed by this methodology. In the F-16 model, this occurs in the g-command mode because it is $a_n = n_z - 1 \approx 0$ in level flight and trimming, i.e., a nonzero F_{long}, is not required at any flight speed. In the q-command mode, the controlled variable is $q - r\tan\chi$ and no stick force is applied either for different flight speeds or for climbing, diving, inverted flight, and steady turns. In the latter situation, the condition $\dot{\theta} = q\cos\chi - r\sin\chi = 0$ implies that $\tan\chi = q/r$. It is only in the α-response mode that trimming is required in all variations of speed and flight-path angle.

Therefore, in g-command and q-command modes, most of the steady states are for the same value of the longitudinal continuation parameter, i.e., F_{long} equal to zero or to the limit value of the command deadband. According to the general technique recalled earlier, this would lead to an infinite number of branches when the equilibrium points are traced as a function of F_{lat} or F_{ped}. In fact, because the local, one-to-one correspondence between the states and the value of the bifurcation parameter along the longitudinal equilibrium branch is no longer retained, we cannot expect that the complete structure of steady states is revealed by the bifurcation diagrams.

Here, we focus on the qualitative analysis of the SCAS behavior in significant operating conditions. To this end, a number of reference flight conditions were determined, having selected the flight speed V, path angle γ, and, in case of steady turning flight, the turn rate Ω. Once the aircraft and SCAS states, the aerodynamic and thrust controls, and the stick and pedal forces at equilibrium are calculated, a starting solution is available for the application of the continuation algorithm. Bifurcation diagrams were traced at different values of the applied thrust δ_T, and we observed that the qualitative behavior of the system was marginally affected by δ_T. As a consequence, the bifurcation analysis discussed in the next section is carried out with F_{long} or F_{lat} as the bifurcation parameters, using one of the following two steady states as starting points: 1) level, symmetric flight with $V = 100$ m s^{-1} and $\delta_T = 0.12$ and 2) level turning flight with $V = 200$ m s^{-1}, $\Omega = 8.7 \times 10^{-2}$ rad s^{-1}, and $\delta_T = 0.28$. Continuation with respect to δ_T is used in only one case to investigate a possible maneuver to recover from deep stall. Finally, steady states computed as a function of F_{ped} are not presented because, due to the ARI, turning flight is commanded by lateral stick inputs, and rudder commands are mainly used for steady sideslip and nose pointing motions, where uncommanded roll rates are prevented by the roll-rate augmentation system.

III. Results

In what follows the steady states of the F-16 model are studied. The altitude is $h = 0$ in all of the considered cases.

The first results, shown in Fig. 3, are for the basic airframe, unaugmented model, where the aft c.g. position at $0.35\bar{c}$ produces, as

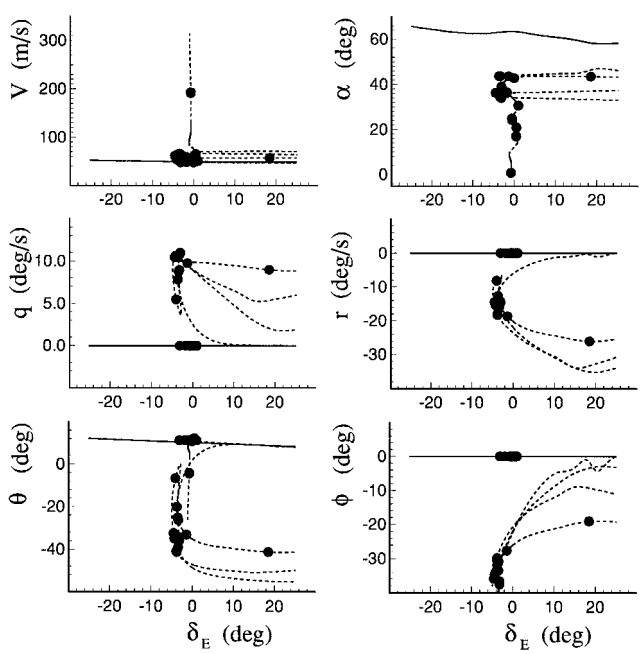

Fig. 3 Steady states of the basic, SCAS-off model vs δ_E; $\delta_A = \delta_R = 0$, $\delta_T = 0.12$: ——, stable and - - - -, unstable; ●, Hopf bifurcation.

we said, a mild longitudinal instability at subsonic speed. Figure 3 shows the continuation diagrams of speed V, angle of attack α, pitch rate q, yaw rate r, pitch angle θ, and roll angle χ vs the stabilator angle, for $\delta_A = \delta_R = 0$. As expected, several unstable segments lie on the branch of symmetrical equilibria due to the negative static margin of the aircraft. It is apparent that small deflections of the stabilator are required for trimming the aircraft, inasmuch as the reduced level of trim drag associated with this characteristic is one of the reasons that led to the choice of flying an unstable aircraft.[8] A second stable branch is visible in the α–δ_E plot for $\alpha \geq 58$ deg and represents the deep-stall steady states that are realized when, at high incidence, the aircraft has static stability and the nose-down stabilator effectiveness is lost. Inadvertent excursions to this range of α are inhibited by the α/a_n limiting system of the augmented aircraft. The lateral steady states are all unstable as the aircraft has good lateral-directional characteristics and, in particular, directional divergences are not to be expected in the full range of angle of attack.[7]

Then, we turn to the complete model with SCAS engaged. Figure 4 shows the bifurcation diagrams of the same states as just described vs the longitudinal control force F_{long}, in α-command mode, for $F_{\text{lat}} = F_{\text{ped}} = 0$. The sideslip angle was very small in all of the continuations due to the actions of both the ARI and the yaw damper and is not reported in the figures. As a first general comment, note that this mode of operation produces a rather conventional steady-state response of the aircraft with a nonzero, positive force stability $\mathrm{d}F_{\text{long}}/\mathrm{d}V$ until the longitudinal command is saturated at $\alpha = 23$ deg.

Also, comparison to Fig. 3 shows that, for the considered aircraft model featuring high augmentation, the steady states present a completely different structure when the SCAS is active. The relevant effect of the SCAS is further revealed by Fig. 5, where the values of α and δ_E at equilibrium with SCAS-on (Fig. 5a) and the steady states of α vs δ_E for the basic airframe model (Fig. 5b) are shown. The two branches of symmetrical equilibria in Fig. 5a are stable, whereas the instability observable for $7.9 \leq \alpha \leq 11.8$ deg is due to a mild directional divergence that drives the aircraft state into one of the two nonsymmetrical, stable equilibrium branches bifurcating from the longitudinal one (χ–F_{long} plot in Fig. 4). Constant values of either α and δ_E (marked by the symbols $\triangle$ and ∇), due to the α limiter providing full nose-down inputs on the stabilator at $\alpha \geq 25$ deg, replace the two branches of deep stall at $40 < \alpha < 46$ and $58 < \alpha < 63$ deg, respectively, shown in Fig. 5b. Finally, as a further effect of the α limiter and the ASPS, the nonsymmetrical equilibria of the basic airframe at $\alpha > 32$ deg are now absent.

The phugoid appears slightly damped in the α-command mode,[13] the pertinent eigenvalue $\lambda = -0.001 \pm 0.13i\ \mathrm{s}^{-1}$. As mentioned, commanded flight conditions at angles of attack higher than 25 deg are not allowed by the α limiter. However, equilibria on the deep stall branch at $\alpha = 58$ deg could be physically realized due to an external disturbance bringing the angle of attack at values higher than 50 deg. In this respect, the response to a step vertical gust of 25 $\mathrm{m\,s}^{-1}$ when flying at an equilibrium, $V_e = 60\ \mathrm{m\,s}^{-1}$ and $\alpha_e = 24$ deg, was simulated and, even at such a low flight speed, the α limiter appeared to prevent the aircraft from entering a deep stall.

Figure 6 shows the steady states of the F-16 vs the lateral control force F_{lat} for $F_{\text{long}} = 22$ N and $F_{\text{ped}} = 0$ N. The starting point for the continuation is a stable equilibrium at $V_e = 100\ \mathrm{m\,s}^{-1}$ and $\alpha_e = 6.8$ deg, on the branch of symmetrical stable steady states of Fig. 4. In the absence of any other control action but F_{lat}, a roll velocity p is commanded by the roll CAS, and the equilibria are for helical paths at increasing velocity and nose-down attitude. Note, in all of the figures, the effect of the sidestick controller deadband. Figure 7 presents pitch and roll angles at equilibrium vs F_{lat} in the α-command mode

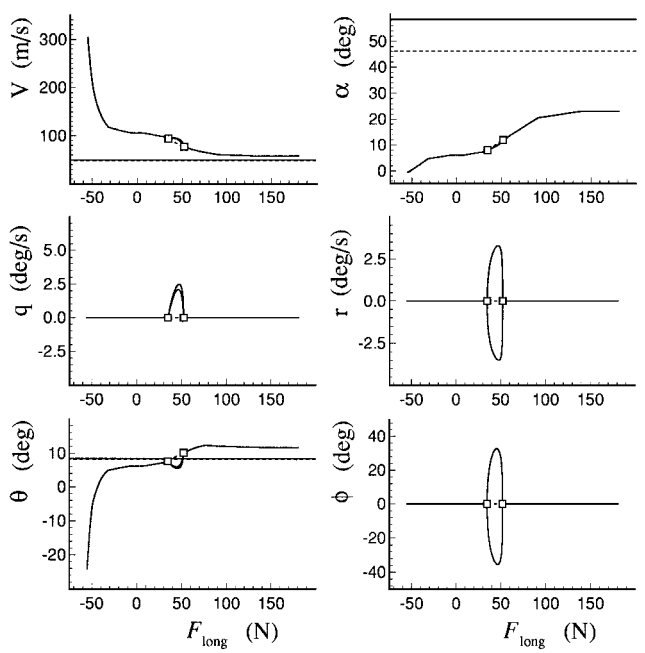

Fig. 4 Steady states vs F_{long}, α-command mode; $F_{\text{lat}} = F_{\text{ped}} = 0$, $\delta_T = 0.12$: ——, stable and - - - -, unstable; □, pitchfork bifurcation.

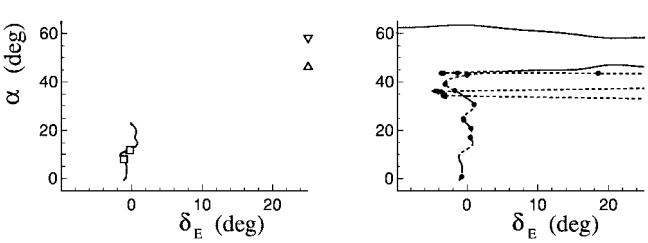

a) SCAS-on in α-command mode **b) Basic airframe**

Fig. 5 Steady state α vs δ_E; $F_{\text{lat}} = F_{\text{ped}} = 0$, $\delta_T = 0.12$: ——, stable and - - - -, unstable; □, pitchfork bifurcation and ●, Hopf bifurcation.

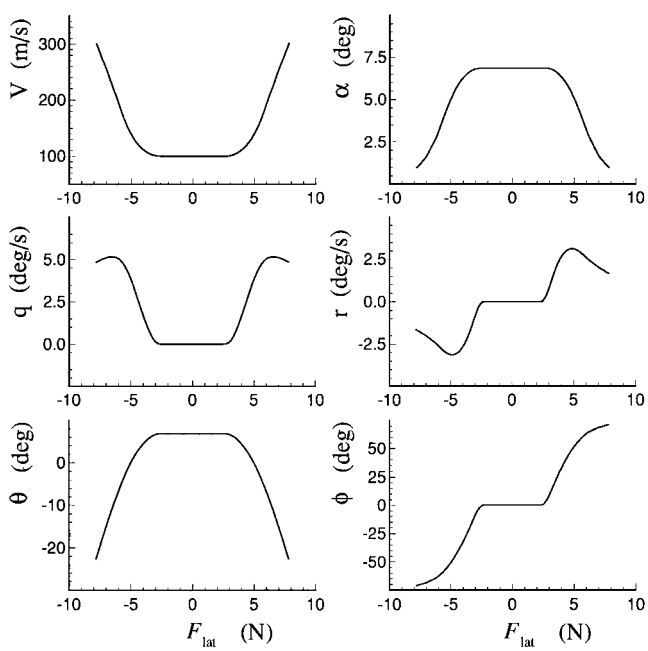

Fig. 6 Steady states vs F_{lat}, α-command mode; $F_{\text{long}} = 22$ N and $F_{\text{ped}} = 0$, $\delta_T = 0.12$: ——, stable and - - - -, unstable.

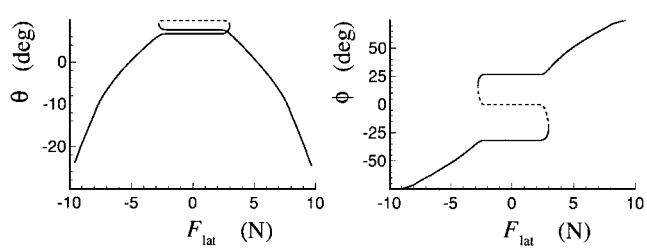

Fig. 7 Steady states vs F_{lat}, α-command mode; $F_{\text{long}} = 50$ N and $F_{\text{ped}} = 0$, $\delta_T = 0.12$: ——, stable and - - - -, unstable.

for a different value of the longitudinal stick force, i.e., $F_{\text{long}} = 50$ N and $F_{\text{ped}} = 0$. The initial point for the continuation is now in the range of F_{long} where, as seen in Fig. 4, the symmetrical steady states are unstable. The hysteresis cycle in the χ–F_{lat} plot determines a jump from positive to negative values of the roll angle as $|F_{\text{lat}}|$ is increased at values higher than 2.7 N. This phenomenon occurs at very low values of the roll velocity when the CAS commands quite small deflections of the ailerons that drive the aircraft into one of the two stable, nonsymmetrical equilibria at $|F_{\text{lat}}| < 2.7$ N.

The steady states vs F_{long} and the longitudinal SCAS for the g-command mode are shown in Figs. 8–10. In particular, Fig. 8 presents the steady states of V, α, θ, and χ as a function of F_{long} for $F_{\text{lat}} = F_{\text{ped}} = 0$. As anticipated in the preceding section, in this SCAS mode, trimming is necessary only in climbing, diving, turning, and inverted flight. In steady symmetric flight, the commanded load factor is $a_{n_e} = \cos\theta_e$ and, consequently, the command gradient $\mathrm{d}F_{\text{long}}/\mathrm{d}a_n$ is very small. We see that when we exclude the deadband region and the saturation of the longitudinal command, the branch of longitudinal equilibria is, in fact, vertical. The lateral equilibria are all unstable.

The same instability is apparent for a segment of the longitudinal branch, when the pitch angle is positive and until the command saturates, and corresponds to an aperiodic divergence in pitch. This behavior can be interpreted with reference to Fig. 9, where a sketch of the longitudinal g-command SCAS appears. When the aircraft is in steady level flight, i.e., $\alpha_e = \theta_e$, $a_{n_e} = g_{\text{com}} + 1$, the SAS produces a nose-down command, as expected, following an increase of α due to some perturbation. However, the CAS sees a positive error signal in the g channel because, during the perturbed motion, the load factor was higher than the unperturbed, reference value. As a result, after the proportional plus integral feedforward of the error, a pitch-down command is demanded, which eventually drives the system back to the equilibrium, at a negative pitch angle, when $a_n = \cos(-\theta_e)$. This divergence is very slow and is eliminated when a pitch autopilot, not included in the present model, is active.

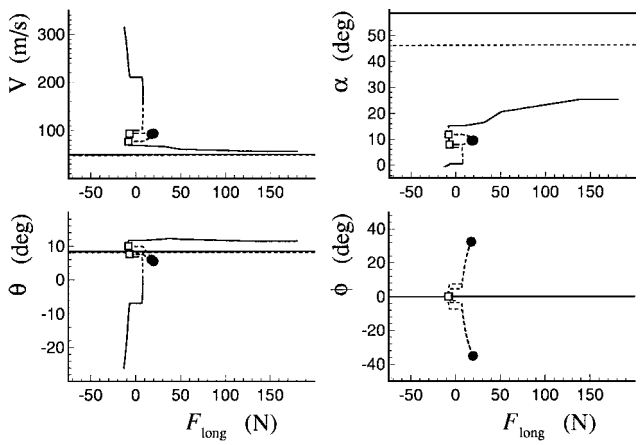

Fig. 8 Steady states vs F_{long}, g-command mode; $F_{\text{lat}} = F_{\text{ped}} = 0$, $\delta_T = 0.12$: ——, stable and - - - -, unstable; □, pitchfork bifurcation and ●, Hopf bifurcation.

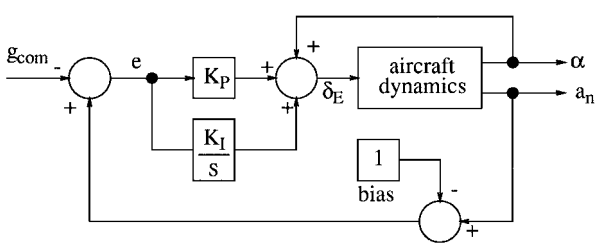

Fig. 9 Longitudinal SCAS in g-command mode.

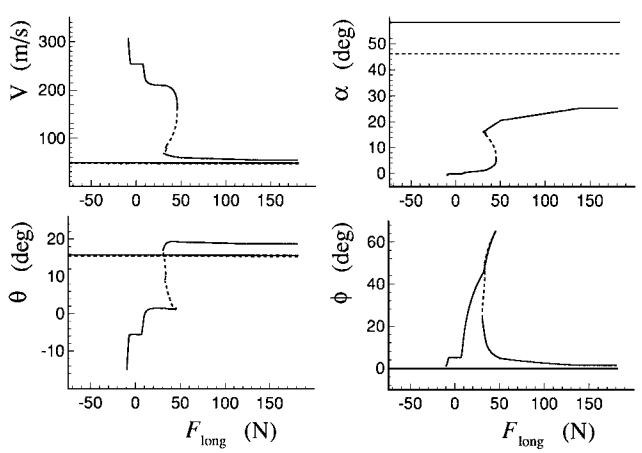

Fig. 10 Steady states vs F_{long}, g-command mode; $F_{\text{lat}} = -2.7$ N, $F_{\text{ped}} = 70$ N, $\delta_T = 0.28$: ——, stable and - - - -, unstable.

In Fig. 10, the steady states are continued as a function of F_{long} for $F_{\text{lat}} = -2.7$ N and $F_{\text{ped}} = 70$ N. In this situation, the starting point for the continuation algorithm, at $F_{\text{long}} = 22$ N, is the steady turn with velocity $V = 200\ \text{m s}^{-1}$. We observe a branch of stable equilibria, for $-10 \le F_{\text{long}} \le 50$ N, corresponding to turns at decreasing radius as higher g are commanded. A second segment of the same branch, for $40 \le F_{\text{long}} \le 180$ N, is related to reduced values of the roll angle as α increases. This behavior is due to the g_{com} vs α scheduling in the SCAS when a reduction of the angle of attack allows for a higher commanded acceleration.[7]

Figure 11 is for the SCAS in q-command mode. The starting condition for the continuation is the same steady turn as the preceding case, with a different control force, i.e., $F_{\text{long}} = 0$. Also, we have $F_{\text{lat}} = -2.7$ N and $F_{\text{ped}} = 70$ N. Significant points on the branch at $\alpha < 25$ deg were numbered to improve the clarity of the plots. In this mode all of the helical flight equilibria are at the limit of the deadband (points 1–5), due to the $q - r\tan\chi$ feedback. The roll angle is brought to zero when the angle of attack saturates (points 5–8), as was already observed in the g-command mode. The equilibria for $6 \le \alpha \le 20$ deg (points 3–5) are unstable as a result of two couples of the Hopf bifurcations. Also unstable are equilibria at very low values of angle of attack (points 1–2). In particular, this very mild divergence is due to the washout in the r channel, the positive eigenvalue being as low as $\lambda = 2 \times 10^{-4}\ \text{s}^{-1}$.

Some results were then obtained by eliminating certain features of the SCAS to investigate the behavior of the vehicle under SCAS failure conditions or, more generally, to carry out a stability analysis of the augmented aircraft in an expanded flight envelope. In this respect, the α-limiter was disengaged and the angle of attack at equilibrium, for the SCAS in the g-command mode, with F_{long} as the continuation parameter and $F_{\text{lat}} = -2.7$ N, $F_{\text{ped}} = 70$ N, shown in Fig. 12. The plot of α vs δ_E is also shown. Comparison to

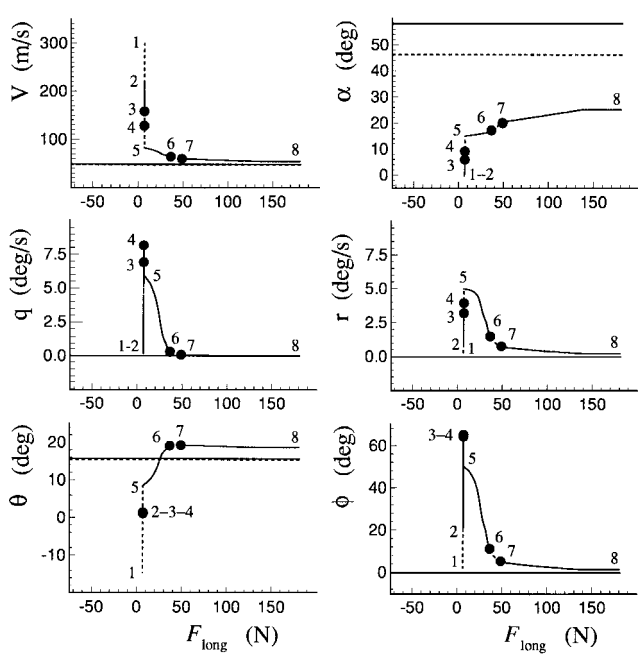

Fig. 11 Steady states vs F_{long}, q-command mode; $F_{\text{lat}} = -2.7$ N, $F_{\text{ped}} = 70$ N, $\delta_T = 0.28$: ——, stable and - - - -, unstable; ●, Hopf bifurcation.

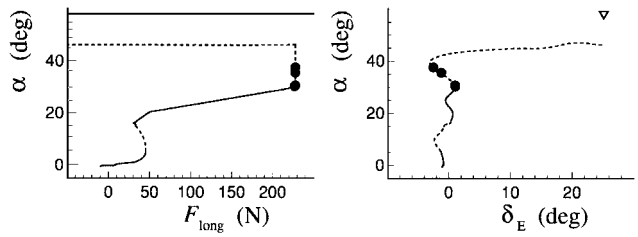

Fig. 12 Steady state α vs F_{long} and δ_E, g-command mode, α limiter disengaged; $F_{lat} = -2.7$ N, $F_{ped} = 70$ N, $\delta_T = 0.28$: ——, stable and - - - -, unstable; ●, Hopf bifurcation.

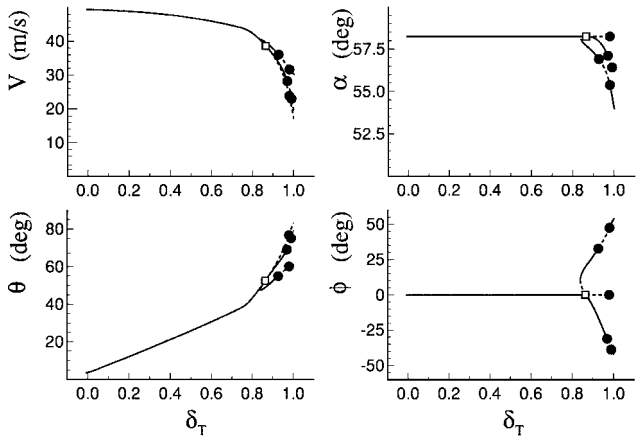

Fig. 13 Steady states vs δ_T, g-command mode, α limiter disengaged; $F_{long} = F_{lat} = F_{ped} = 0$: ——, stable and - - - -, unstable; □, pitchfork bifurcation and ●, Hopf bifurcation.

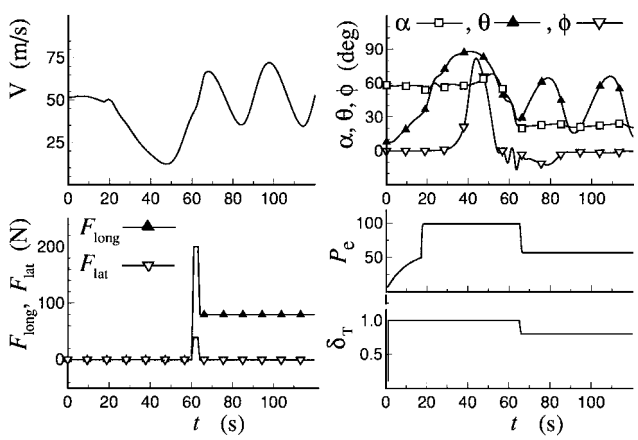

Fig. 14 Simulation of recovery from deep stall.

the α plot of Fig. 10 shows that, for $F_{long} \leq 130$ N, the branch of equilibria in steady turns is not modified, whereas the steady states on the two branches at $\alpha > 45$ deg can now be reached by either external disturbances or pilot inputs. In particular, the saddle-node bifurcation that occurs at $F_{long} = 227$ N, not present when the α limiter is on, is responsible for the aircraft entering a deep stall. As for the stable branch at $\alpha = 58$ deg, we observe that the vehicle remains in deep stall due to the negligible control power of the stabilator at that incidence,[7] although the α feedback of the SAS is still commanding full nose down, as shown in the α–δ_E plot of Fig. 12, where the symbol ∇ marks the constant value of α and δ_E along the branch. Note also that the nonsymmetrical equilibria shown in Figs. 3 and 5b are not allowed, even with the α limiter disengaged, because for $\alpha > 30$ deg the ASPS prevents any buildup of yaw rate.

In Fig. 13, the thrust level δ_T is the continuation parameter. In the absence of the α limiter, this case was considered to identify a possible maneuver to recover from the deep stall. As the thrust is increased, the aircraft pitches up, the symmetric equilibrium becomes unstable, and the state is attracted by a lateral roll condition at decreasing angle of attack. Finally, Fig. 14 shows an attempted recovery, based on the preceding discussion. The governing equations were numerically integrated by a fourth-order Runge–Kutta algorithm, with constant step size $\Delta t = 1/32$ s. At the initial time, the F-16 has $V_e = 53$ m s^{-1} and $\alpha_e = 58$ deg. After maximum thrust is applied, the pitch angle increases, and at $t = 45$ s, the state jumps into a nonsymmetrical flight condition at a roll angle $\chi = 70$ deg. Then, both α and χ decrease, and at $t = 60$ s, a longitudinal command is effective in further reducing the angle of attack to a value as low as 20 deg, whereas a lateral command drives the aircraft back into symmetric flight.

IV. Conclusion

The application of bifurcation theory to the analysis of highly augmented aircraft models presents several aspects of interest. The SCAS tailors the dynamic behavior of the vehicle to a great extent, particularly when the basic, unaugmented model possesses a negative static stability. The technique maintains its effectiveness in this kind of application, allowing for an efficient analysis and characterization of the complete, high-order differential system associated to the SCAS on aircraft model. The presented results show that the dynamical characteristics related to the handling qualities of an aircraft featuring, to a certain extent, superaugmentation are correctly reproduced and identified.

On the other hand, the complete structure of the equilibrium solutions of the system cannot be revealed because the aerodynamic control angles are dynamical states that vary in a rather complex manner as a function of the control forces for each of the SCAS modes of operation. Also, in most steady flight situations, no trimming is required and this, again, limits the available information, in terms of stability characterization of as many equilibrium points as possible, when entire branches of steady states are associated to a zero value of the control force.

Acknowledgment

This work was partially supported by the Italian National Research Council.

References

[1]Guckenheimer, J., and Holmes, P., *Nonlinear Oscillations, Dynamical Systems and Bifurcations of Vector Fields*, Springer–Verlag, New York, 1983, pp. 1–60, 117–156.

[2]Doedel, E. J., and Kervenez, J. P., *Software for Continuation Problems in Ordinary Differential Equations with Applications*, California Inst. of Technology, Pasadena, CA, 1985, pp. 7–56, 121–217.

[3]Jahnke, C. C., and Culick, F. E. C., "Application of Bifurcation Theory to the High-Angle-of-Attack Dynamics of the F-14," *Journal of Aircraft*, Vol. 31, No. 1, 1994, pp. 26–34.

[4]Carrol, J. V., and Mehra, R. K., "Bifurcation Analysis of Nonlinear Aircraft Dynamics," *Journal of Guidance, Control, and Dynamics*, Vol. 5, No. 5, 1982, pp. 529–536.

[5]Planeaux, J. B., Beck, J. A., and Baumann, D. D., "Bifurcation Analysis of a Model Fighter Aircraft with Control Augmentation," AIAA Paper 90-2836, Aug. 1990.

[6]"Handling Qualities of Unstable Highly Augmented Aircraft," AGARD Working Group WG-17, AGARD-AR-279, May 1991, pp. 1–18.

[7]Nguyen, L. T., Ogburn, M. E., Gilbert, W. P., Kibler, K. S., Brown, P. W., and Deal, P. L., "Simulator Study of Stall/Post-Stall Characteristics of a Fighter Airplane with Relaxed Longitudinal Static Stability," NASA TP-1538, Dec. 1979.

[8]Droste, C. S., and Walker, J. E., *The General Dynamics Case Study on the F-16 Fly-By-Wire Control System*, AIAA Professional Study Series, AIAA, New York, 1979, pp. 1–20.

[9]Marchand, M. A., "Pitch Rate Flight Control System for the F-16 Aircraft to Improve Air-to Air Combact," U.S. Air Force Inst. of Technology, AFIT/GGC/EE/77-7, Wright–Patterson AFB, OH, Dec. 1977, pp. 1–61.

[10]McRuer, D., Johnston, D., and Myers, T., "A Perspective on Superaugmented Flight Control: Advantages and Problems," *Journal of Guidance, Control, and Dynamics*, Vol. 9, No. 5, 1986, pp. 530–540.

[11]Press, W. H., Flannery, B. P., Teukolsky, S. A., and Vetterling, W. T., *Numerical Recipes—The Art of Scientific Computing*, Cambridge Univ. Press, Cambridge, England, UK, 1986, pp. 77–101.

[12]"IMSL Math/Library, FORTRAN Subroutines for Mathematical Applications," Version 1.1, International Mathematical and Statistical Libraries, Houston, TX, Aug. 1989, EIGRF-1–EIGRF-4.

[13]Gibson, J. C., "Handling Qualities for Unstable Combat Aircraft," *Proceedings of the 15th Congress of the International Council of the Aeronautical Sciences* (London), International Council of the Aeronautical Sciences and AIAA, New York, 1986, pp. 433–445 (Paper ICAS-86-5.3.4).